



Forecasting the Heights of Later Waves in Pacific-Wide Tsunamis

HAROLD O. MOFJELD*, FRANK I. GONZÁLEZ, EDDIE N. BERNARD
and JEAN C. NEWMAN

NOAA/Pacific Marine Environmental Laboratory, 7600 Sand Point Way NE, Seattle, Washington

(Received: 9 February 1999)

Abstract. A method is derived to forecast the extreme heights of later waves in Pacific-wide tsunamis, for locations in the vicinity of real-time reporting tide gages. The forecast for wave peaks has the form $\eta_F(t) = \eta_B(t) + \eta_e(t)$, where $\eta_e = A\sigma \exp[-(t - t_o)/\tau]$. Here, the forecast begins at time $t = t_o$, which is 4 h after tsunami detection at a tide gage, σ is the standard deviation of tsunami-band fluctuations observed in the 2-h time interval before the forecast begins, η_B is a background water level prediction that includes the tides and lower frequency oscillations, $\tau = 48$ h is an e-folding decay constant, and $A = 3.0$ is a constant coefficient. Placing a minus sign in front of η_e provides a forecast for wave troughs. This form for the forecast, and the values of the parameters, are justified using probability theory and Monte Carlo simulations based on 3000 synthetic tsunami time series. The method is then tested successfully (i.e., agreement within 0.5 m) against six past Pacific-wide tsunamis, as observed at U.S. tide gages. These case studies include the five major tsunamis to produce loss of life and/or substantial damage to U.S. coastal communities during the Twentieth Century. The sixth study is the 1994 Shikotan tsunami, which is the latest Pacific-wide tsunami to trigger tsunami warnings for U.S. regions. Algorithms for detecting local tsunami onset and generating forecasts are given in an appendix, together with a description of the wavelet method used to generate the synthetic tsunami series.

Key words: short-term tsunami forecasting, Pacific-wide tsunamis, exponential tsunami decay, statistical modeling.

1. Introduction

Pacific-wide tsunamis remain dangerous for many hours (Mofjeld *et al.*, 1999). Later tsunami waves threaten rescue and recovery operations, especially when they arrive at high tide. Such waves also endanger vessels in shallow water. For these reasons, emergency managers need wave height forecasts to help guide rescue and recovery operations. They also need them to decide when to issue the all-clear. In this paper, we present a method to make such forecasts for sites near real-time reporting tide gages. The goal is to provide an adequate forecast as soon as possible following the local onset of a tsunami.

* *Address for correspondence:* Pacific Marine Environmental Laboratory, National Oceanic and Atmospheric Administration, Building 3, 7600 Sand Point Way N.E., Seattle, WA 98115, U.S.A., e-mail: mofjeld@pmel.noaa.gov

The forecast method is based on a study of observed Pacific-wide tsunamis (Mofjeld *et al.*, 1997b). It shows that an amplitude envelope can be computed from tide gage observations which encompasses the next tsunami wave. The total envelope η_F is the sum of the background water level η_B (primarily the tides) and a wave envelope η_e

$$\eta_F = \eta_B + \eta_e; \eta_e = A\sigma. \quad (1)$$

Here, σ is the standard deviation of the tsunami-band fluctuations preceding the wave. The study shows that setting the empirical coefficient A equal to ~ 3.0 – 3.5 produces envelopes which closely match the maximum wave heights. Replacing the plus sign in (1) with a minus sign leads to an envelope for the wave troughs.

In the present paper, we extend the forecast (1) to the remainder of Pacific-wide tsunamis by assuming that their amplitudes decay exponentially in time (Figure 1). The form is based on studies of how these tsunamis decay (Miller *et al.*, 1962; Van Dorn, 1984, 1987). Specifically, Van Dorn (1984) shows that following the first day of Pacific-wide tsunamis, their energy decays with an e-folding time constant of about 22 h. He finds this to be true for a variety of tsunamis and impact sites. Hence, the characteristics of this decay are general properties of the Pacific Basin. Based on analyses of past tsunamis, we will show that the forecast method is able to generate reasonable predictions (within 0.5 m) when only 4 h has passed since the local tsunami onset. Since the exponential decay time for tsunami energy is about 1 day, the decay time for wave amplitude is about 2 days (twice the energy's). We will use an amplitude decay time of 48 h.

Figure 2 illustrates the steps leading to a forecast. After the initial detection of a tsunami, σ is computed from a 2-h data segment that follows the first wave group. This is to avoid any unique characteristics of the first waves that are non-representative of the later waves in the tsunami. In Figure 2, the forecast is seen to track the maximum wave heights as the background water level rises toward the next high tide.

In the next section, we use probability theory to rigorously define the forecast amplitude envelopes bounding the later tsunami waves. It is essential that the forecast method be insensitive to tsunami wave frequency, because real tsunamis are made up of fluctuations within a range of frequencies that are likely to shift with time (e.g., Figure 2). Monte Carlo analyses using 3000 synthetic tsunamis demonstrate this feature of the method. These analyses also determine the minimum data segment needed to provide an adequate estimate of standard deviation σ . The probability theory and simulations verify that $A = 3.0$ is an appropriate value for this coefficient. Section 3 discusses ways of estimating the background water levels, used both to estimate σ and as a contribution to the total wave height.

Section 4 shows the application of the forecast method to five major tsunamis that have struck U.S. coastal communities during the Twentieth Century. The examples are based on tide gage observations at Crescent City, on the Northern Coast of California, and two sites in Hawaii: Honolulu and Hilo. The case studies also

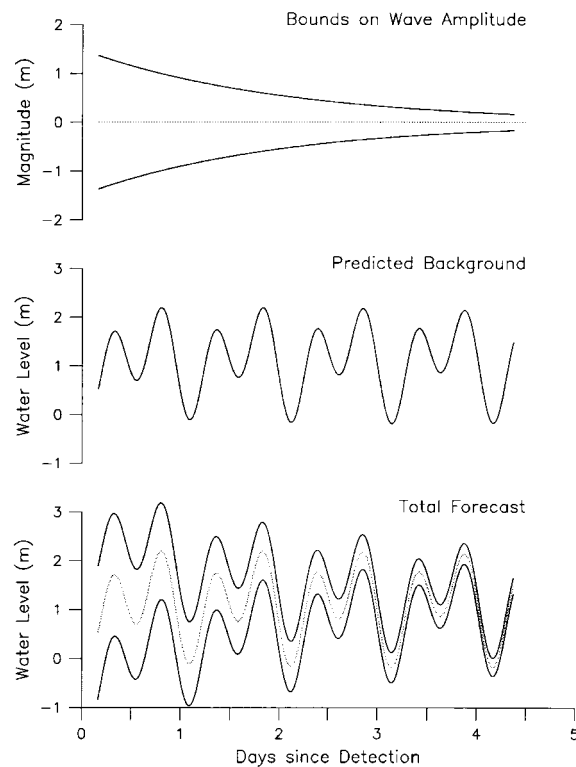


Figure 1. Tsunami wave height forecast, shown schematically as the sum of exponentially decaying wave envelopes and a time-varying background water level.

include the 1994 Shikotan tsunami as observed in Alaska, the U.S. West Coast and Hawaii. This is the latest Pacific-wide tsunami to trigger tsunami warnings for sections of the U.S. Coast.

Section 5 discusses emerging research that will provide forecasts for the gap in time between the onset of a tsunami and the beginning of the forecast presented in this paper. It also discusses the need for research to extend the method to locally generated tsunamis and to sites away from the vicinity of tide gages. This section is followed by the conclusions of the work. The Appendix contains descriptions of automated algorithms for the forecast method and the wavelet method used to generate the synthetic tsunami time series.

2. Probability Theory

In this section, we derive a forecast for envelopes bounding the maximum heights of later waves in Pacific-wide tsunamis. It is convenient to temporarily set the background water level η_B to zero in order to focus on the tsunami waves. In the first part of the section, the tsunami waves are assumed to be realizations of a stationary random process. Monte Carlo simulations are used to analyze the behavior of the

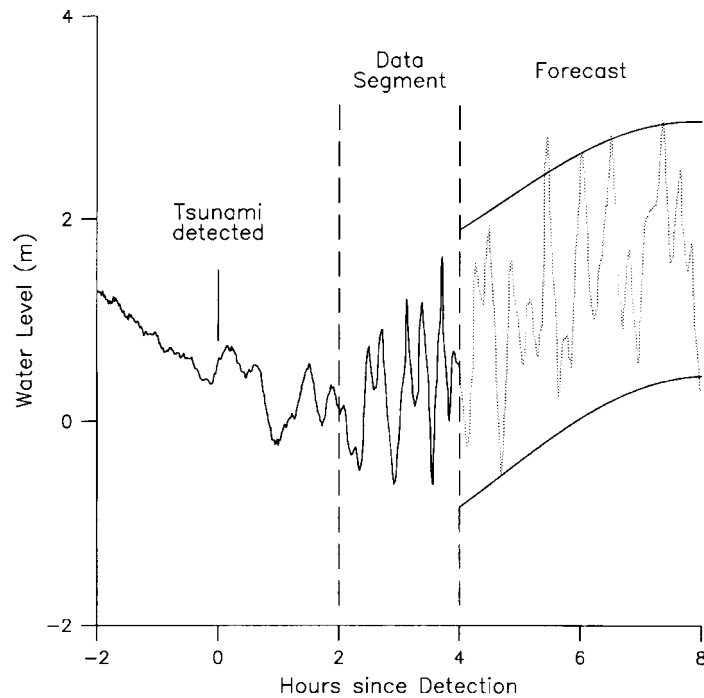


Figure 2. Early stages of a tsunami, showing time of tsunami detection, data segment used to compute wave envelopes, and the first few hours of the tsunami wave height forecast. Example is for the 1960 Chile tsunami as observed at Crescent City, California.

larger waves in a tsunami series, as functions of dominant tsunami wave period and the length of the data series used to estimate the standard deviation σ . Later in the section, we extend the forecast method to tsunamis that decay exponentially in time.

2.1. DEFINITION OF THE WAVE HEIGHT ENVELOPE

During the forecast period, each wave peak may be regarded as an attempt to exceed a given height η . If $p(\eta)$ represents the average probability of a wave peak exceeding η , then the probability that k or more waves will exceed η is given by the cumulative binomial distribution $Q_k(p|N)$, where N is the total number of wave peaks that occur during the forecast period. As we shall see, the probability Q_k is substantial (Figure 3) for $k = 1$ but small for $k \geq 3$ when: (a) $0.005 \leq p \leq 0.02$ and (b) N corresponds to wave periods of 5–60 minutes and forecast lengths of 2–6 h (Table I). This range of p allows the forecast envelope to encompass almost all the wave peaks, without being unrealistically large.

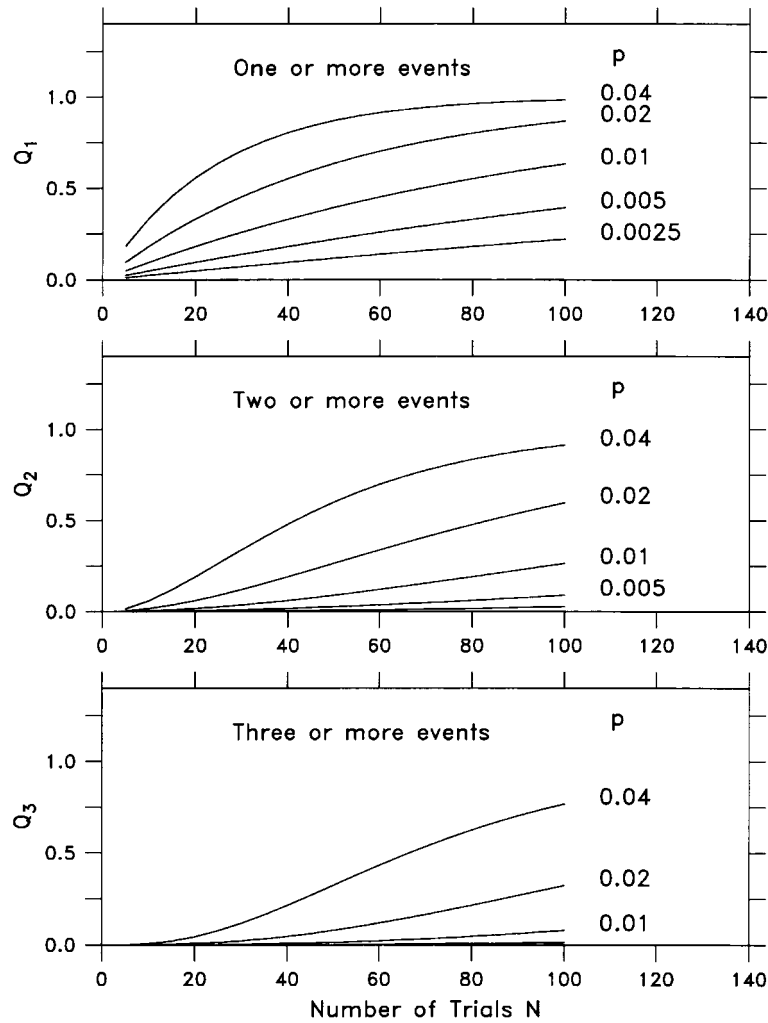


Figure 3. The cumulative binomial distribution $Q_k(p|N)$ giving the probability of k or more events (i.e., tsunami wave peaks exceeding a height η) in N trials, where $p(\eta)$ is the probability of occurrence per trial.

As a measure of how much a wave peak might exceed a threshold height η , we define the envelope η_e to be the expectation height for those peaks exceeding η ,

$$\eta_e = \int_{\eta}^{\infty} \eta' p(\eta') d\eta' / Q'(\eta); \quad Q' = \int_{\eta}^{\infty} p'(\eta') d\eta'. \quad (2)$$

Here, $p'(\eta')$ is the probability density function (pdf) for the wave heights. Setting the cumulative probability $Q'(\eta) = p$ determines the height η , and thence η_e . While there is a finite probability that a wave may exceed η_e by a substantial amount, this probability decreases very rapidly with height for the Gaussian

Table I. Number of tsunami wave peaks at different frequencies (identified by wave period) and lengths of time series. Bold type indicates ≥ 6 peaks

Period (min)	Series length (h)		
	2	4	6
5	24	48	72
10	12	24	36
20	6	12	18
40	3	6	9
60	2	4	6

pdf. We will see in Section 4 that this is also the case for observed Pacific-wide tsunamis.

To relate η_e to the standard deviation σ , we use an argument based on the linear scaling between wave heights and σ . Since σ is computed from n discretely sampled data values η_i ,

$$\sigma = \text{Var}^{1/2}, \quad \text{Var} = \frac{1}{n} \sum_{i=1}^n \eta_i^2; \quad (3)$$

a constant factor multiplying the data $\{\eta_i\}$ becomes a factor multiplying σ . This can also be thought of as a result of dimensional analysis, where the coefficient A is dimensionless. Hence, we can take as our forecast of the maximum wave heights

$$\eta_e = A\sigma. \quad (4)$$

Note that this is the same expression for η_e as occurs in the empirical formula (1).

Using wavelet simulations (described in the Appendix), we relate the average probability p of a wave exceeding the forecast to the coefficient A . For simplicity, we assume that data and forecast periods contain approximately the same number of tsunami waves. The following logarithmic relationship closely fits the results of the numerical simulations (Figure 4),

$$A = a_0 - a_1 \log_{10}(p), \quad (5)$$

Table II shows that the coefficients a_0 and a_1 depend only weakly on the number of wave peaks in the forecast period, supporting the idea of using a single coefficient A for the expected range of tsunami wave periods.

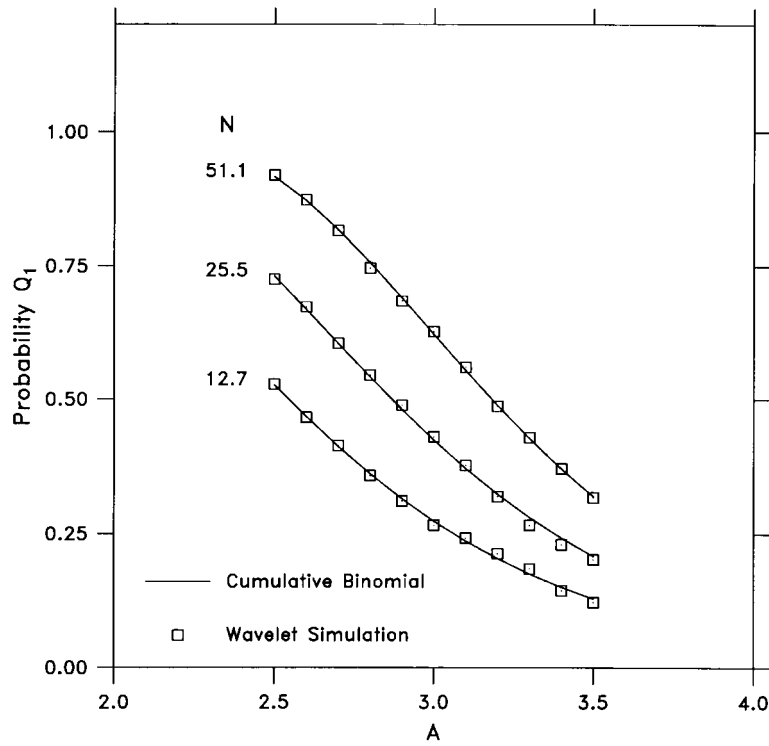


Figure 4. Fit of the cumulative binomial distribution Q_1 to exceedance probabilities derived from Monte Carlo analyses of synthetic tsunamis; done for three different frequency bands indicated by the average number of wave peaks in the forecast segment.

Table II. The parameters a_0 and a_1 based on fits of the cumulative binomial probability Q_1 (one or more exceedances) to synthetic tsunami time series. Values are given as functions of the average number N of wave peaks in the forecast period, using 1000 synthetic tsunamis in each frequency band

N	a_0	a_1
12.7	0.74	1.45
25.5	0.78	1.33
51.1	0.81	1.26

Table III. Height η_e and the ratios to η_e of the average peak height $\bar{\eta}$ and threshold amplitude η , given as functions of the coefficient A . Values are based on analysis of synthetic tsunami time series with $\sigma = 1$ and an average height of the $N = 51.1$ wave peaks in the forecast period

A	η_e	$\bar{\eta}/\eta_e$	η/η_e
2.5	3.0	0.40	0.84
3.0	3.4	0.34	0.87
3.5	3.9	0.30	0.90

Choosing a range 0.005–0.02 for the probability p fixes the range of the coefficient A at 2.5–3.5. In this range, the numerical value of η_e (Table III) increases essentially linearly with A . For $A = 3.0$, η_e is approximately three times the average wave height $\bar{\eta}$ but only 13% larger than the threshold η . Hence, this is an appropriate value for the coefficient A .

2.2. FULL-DURATION FORECASTS

The full-duration forecasts (e.g., Figure 1) are based on background water levels, an initial estimate of wave amplitude η_o and an exponential decay factor. Letting $\eta_o = A\sigma$ be the initial height and t_o be the start of the forecast, the forecast for the remainder of the tsunami is then

$$\eta_F(t) = \eta_B(t) + \eta_o \exp[-(t - t_o)/\tau], \quad (6)$$

where $\eta_o = A\sigma$, $A = 3.0$, t_o is the start of the forecast, and $\tau = 2$ days. The temporal variations in the background water level $\eta_B(t)$ are primarily due to the changing tides. A forecast for the lowest water levels is obtained by substituting $-\eta_o$ for $+\eta_o$.

Because tsunami wave periods (e.g., Table I) are much less than the e-folding time of 2 days, the statistics of the tsunami waves are quasi-steady (i.e., locally stationary). Hence, the analysis for stationary processes holds approximately for slowly decaying tsunamis.

3. Background Water Levels

Along the U.S. West Coast and British Columbia, background water levels are large enough (Table IV) to strongly influence the heights reached by tsunamis (e.g., Mofjeld *et al.*, 1997a). This is also true along the coast of Alaska and in the Aleutian Islands. The heights of subtidal fluctuations increases northward along

Table IV. Mean diurnal tidal ranges at selected sites in Alaska, Hawaii, and the Pacific coasts of Canada and the United States. Values are taken from the 1998 NOAA Tide Tables

Location	Range (m)	Location	Range (m)
<i>Alaska</i>		<i>U.S. West Coast</i>	
Kodiak	2.7	Neah Bay, WA	2.4
Seward	3.2	South Beach, OR	2.5
Yakutat	3.1	Crescent City, CA	2.1
Sitka	3.0	San Francisco, CA	1.8
<i>British Columbia</i>		Port San Luis, CA	1.7
Prince Rupert	5.3*	San Diego, CA	1.7
Queen Charlotte	5.4*	<i>Hawaii</i>	
Tofino	2.7	Honolulu	0.6
		Hilo	0.7

*Mean Spring.

the West Coast, e.g., ranging from 0.3 m at Monterey to 0.9 m at Queen Charlotte (Mofjeld *et al.*, 1997). They are due to the superposition of storm-scale, seasonal, and interannual (e.g., El Niño) fluctuations. While the tides and subtidal fluctuations are relatively small in Hawaii, wind waves and swell can be high at exposed sites. Fortunately, the National Weather Service forecasts the heights of wind waves and swell for many locations.

The astronomical tides can be accurately predicted at a tide gage. Water level fluctuations at lower period occur primarily at periods =10 days (e.g., Mofjeld, 1992; Percival and Mofjeld, 1997). These subtidal fluctuations are slowly changing processes that do not change significantly during a tsunami, unless it coincides with a storm event. Hence, these fluctuations can be approximated during the forecast period by the average water level for the preceding 24-h period. Forecasts of storm surge should be included during winter storm and hurricane seasons. Subtracting the tides and subtidal heights from observations provides the tsunami-band data needed to compute the standard deviation σ , and thence η_o in (6).

4. Case Studies

This section compares wave height forecasts with tide gage observations of past Pacific-wide tsunamis. The first part of the section is devoted to major tsunamis (Table V and Figures 5 and 6) that have caused loss of life and/or substantial damage to U.S. coastal communities. The tsunami time series were digitized from analog marigrams by W. Van Dorn, who made them available to the authors. This is with the exception of the 1946 and 1957 tsunamis at Crescent City, which were di-

Table V. Information about five earthquakes that caused major Pacific-wide tsunamis and the maximum runup of these tsunamis at Crescent City, Honolulu and Hilo, as reported by Lander and Lockridge (1989). Earthquake magnitudes are from Pacheco and Sykes (1992); magnitudes inside parentheses are from the NEIS Catalog

Earthquake:	Apr. 1, 1946 E. Aleutian	Nov. 4, 1952 Kamchatka	Mar. 9, 1957 C. Aleutian	May 22, 1960 Chile	Mar. 28, 1964 Alaska
Latitude:	53.3°N	52.8°N	51.6°N	38.2°S	61.1°N
Longitude:	163.2°W	175.4°E	175.4°W	73.5°W	147.6°W
Mechanism:	Normal	Thrust	Thrust	Thrust	Thrust
Magnitude Ms:	7.3 (7.3)	8.2 (8.5)	8.1 (8.6)	8.5 (9.5)	8.4 (8.5)
Impact site	Maximum tsunami runup (m)				
Crescent City, CA	0.9	1.0	1.0	Not listed	4.3
Honolulu, HI	0.6	1.3	1.0	0.8	0.5
Hilo, HI	8.1	2.4	3.9	10.7	3.0

gitized at PMEL. To initiate the forecast procedure, the tsunami detection threshold was set equal to 0.3 m; the detection algorithm is given in the Appendix.

The second part focuses on the 1994 Shikotan tsunami, which is the latest Pacific-wide tsunami to trigger tsunami warnings for sections of the U.S. coast. Although it was highly destructive in the Kuril Islands and Japan, it did not cause significant damage to U.S. coastal regions. However, the tsunami was observed at a large number of U.S. tide gages. It was recorded every 15 seconds on solid state memory devices that were specially installed by the National Ocean Service (NOS) to support tsunami research. A few days after the 1994 event, the devices were removed by tidal observers and mailed to the NOS/Pacific Operations Group for processing. The Group then provided the data to PMEL for analysis and interpretation. Fifteen-second data are not available from the Crescent City and Hilo gages, although the 6-minute data from these gages do show the tsunami. The time series for Kahului, Hawaii, was obtained from a gage maintained by the U.S. Army Corps of Engineers (McGehee and McKinney, 1997). The detection threshold was set to various values in order to initiate the forecasting procedure.

4.1. MAJOR PACIFIC-WIDE TSUNAMIS

The forecasts in Figure 6 are seen to match later waves of the major Pacific-wide tsunamis within 0.5 m. Further, the agreement improves as the tsunamis decay in time. Whether a forecast tends to overestimate, match, or underestimate the extreme waves depends on the heights of the tsunami waves (Figure 6) during the data segment used to compute σ . At Honolulu and Hilo, the first tsunami waves tend to be substantially larger than those following a few hours later. Hence, the

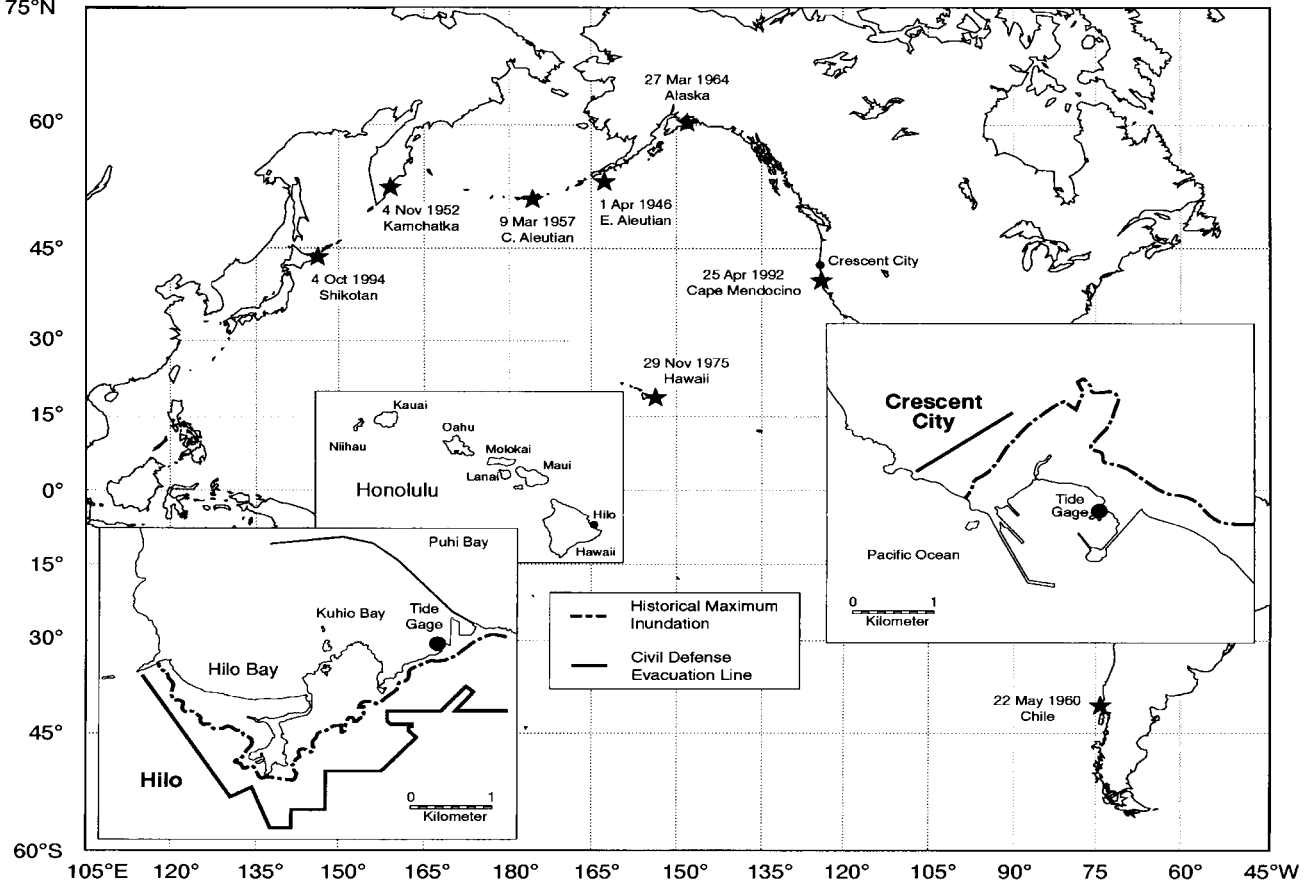


Figure 5. Map of the Pacific Ocean, showing earthquake epicenters of the Pacific-wide tsunamis used in this paper. Also shown are harbor maps for Crescent City, California, and Hilo, Hawaii.

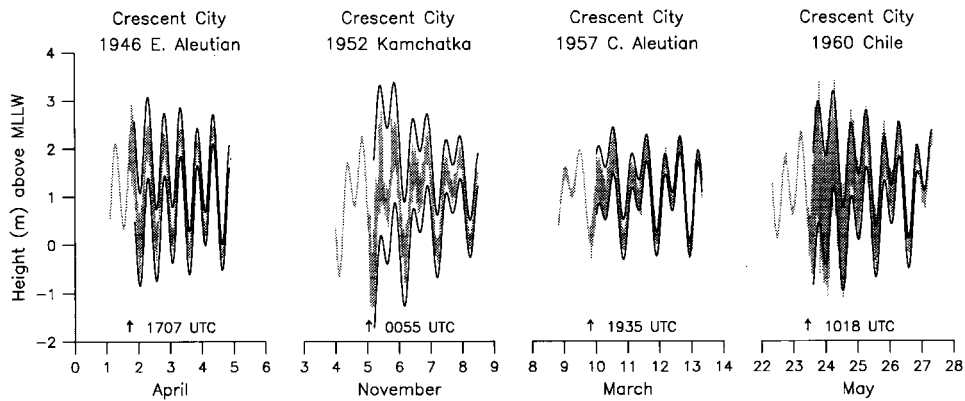


Figure 6a. Wave height forecasts and tide gage observations for major Pacific-wide tsunamis at Crescent City, California. The 1964 Alaska tsunami is not shown because the initial waves of that tsunami destroyed the Crescent City gage.

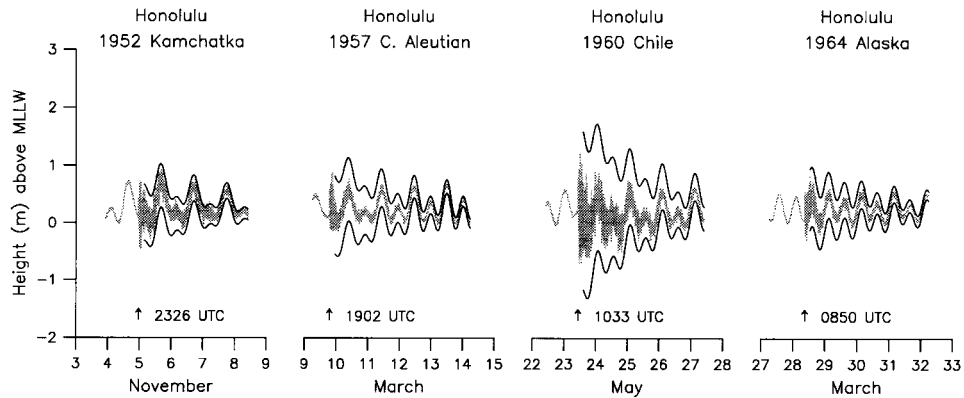


Figure 6b. Wave height forecasts and tide gage observations for major Pacific-wide tsunamis at Honolulu, Hawaii. The 1964 E. Aleutian tsunami is not shown because the background water level series is highly distorted.

forecasts there tend to overestimate the later wave heights. Conversely, the early waves of tsunamis at Crescent City tend to increase with time, causing the forecasts to occasionally underestimate the extreme wave heights. However, a forecast based on the height of the first two or three tsunami waves (e.g., Figure 2) would grossly underestimate the maximum wave heights that occurred a few hours later.

As time proceeds during a tsunami, the forecasts could be improved somewhat by using a longer data segment to compute σ . For example, the overestimates (Honolulu and Hilo) and underestimates (Crescent City) can be largely eliminated by basing the forecasts on 7 h of data; such forecasts then begin 9 h after local tsunami detection. However, starting the forecast 4 h since local tsunami onset gives an adequate forecast as soon as possible. In particular, it is important to issue a forecast before the next high tide. Also, staying with the earlier forecast

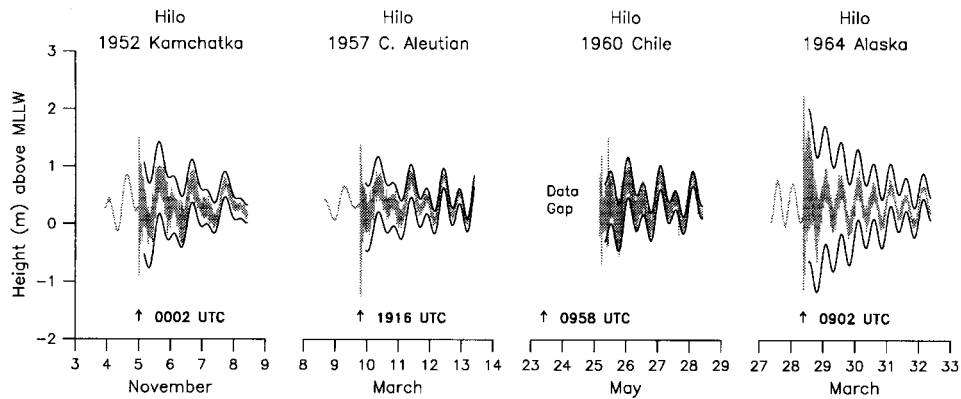


Figure 6c. Wave height forecasts and tide gage observations for major Pacific-wide tsunamis at Hilo, Hawaii. Observations of the 1946 E. Aleutian tsunami are not available for Hilo. The initial waves of the 1960 Chile tsunami damaged the tide gage at Hilo, causing an 18-h data gap that ended when the gage was put back into operation.

eliminates the confusion that will arise if more than one forecast is issued within a few hours.

4.2. SHIKOTAN TSUNAMI

The 1994 Shikotan tsunami was generated on October 4th by a magnitude M_s 8.1 earthquake that occurred northeast of Hokkaido, Japan (Figure 5). The earthquake mechanism was complex and continues to be the subject of active research (e.g., Tanioka *et al.*, 1995; Cummins *et al.*, 1998; Mofjeld *et al.*, 1999).

The forecasts for the Shikotan tsunami (Figures 7 and 8) closely match extreme heights of later waves at most stations. The forecast for Kahului does overestimate the later wave heights at Kahului by about 0.3 m. However, the harbor at Kahului, like Hilo, is subject to swell and wind waves that increase effective amplitudes of tsunami waves. Because standard tide gages do not measure swell and wind waves, these high-frequency waves are not included in the tsunami forecast. Hence, it is not necessarily detrimental that the forecast method produces modest overestimates of tsunami wave heights in these harbors.

Overall, there is close agreement (Figure 8) between the forecast and observed wave amplitudes of the 1994 Shikotan tsunami, even though the frequency distribution varies considerably between regions (Mofjeld *et al.*, 1997b). This result supports the theoretical result in Section 2 that the forecasts are insensitive to tsunami wave frequency. It is important that the forecasts bound the larger waves which appear suddenly when the waves appear to have decayed to low amplitude. Examples of such larger waves can be seen at Port San Luis and Kahului.

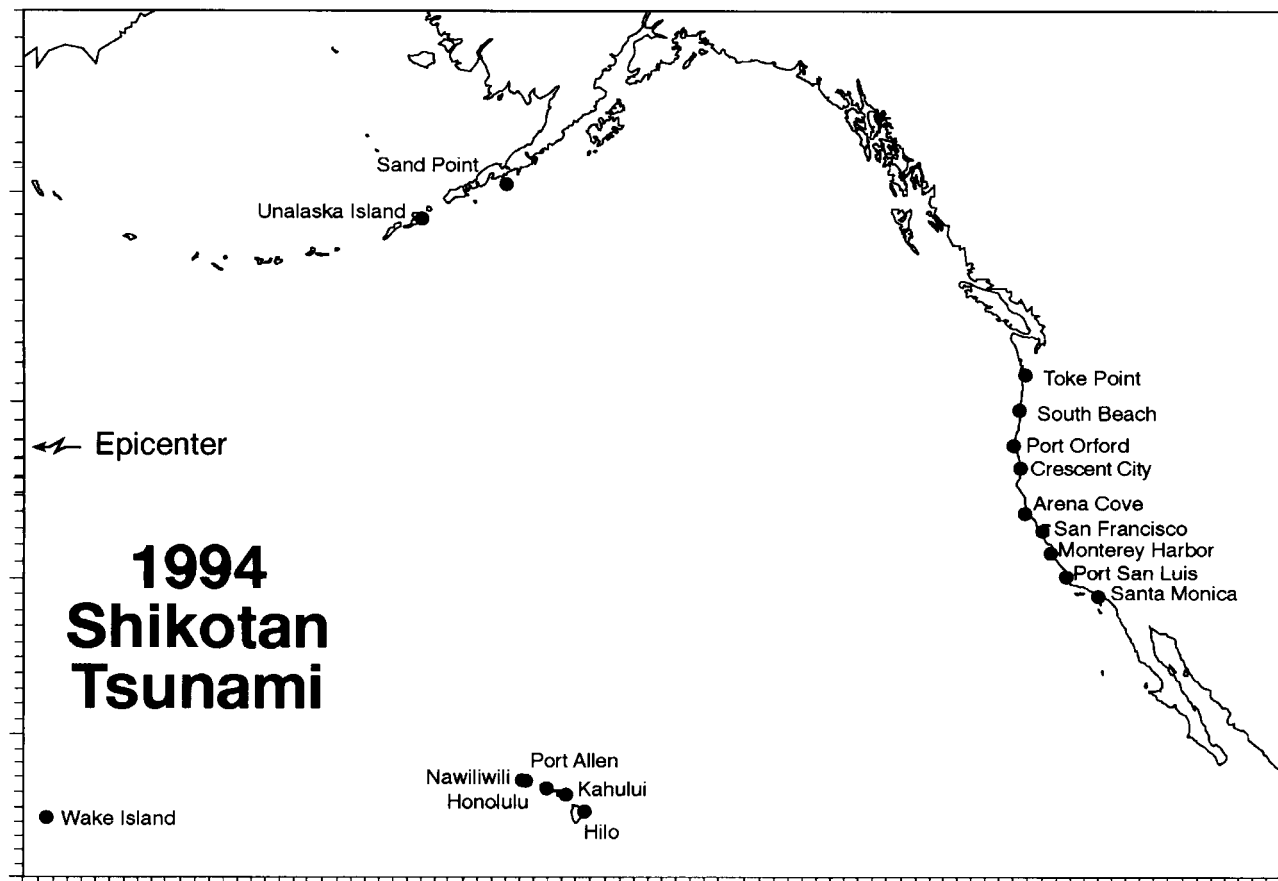


Figure 7. Map of the Northeast Pacific showing selected U.S. tide gage locations where the 1994 Shikotan tsunami was observed.

1994 Shikotan Tsunami

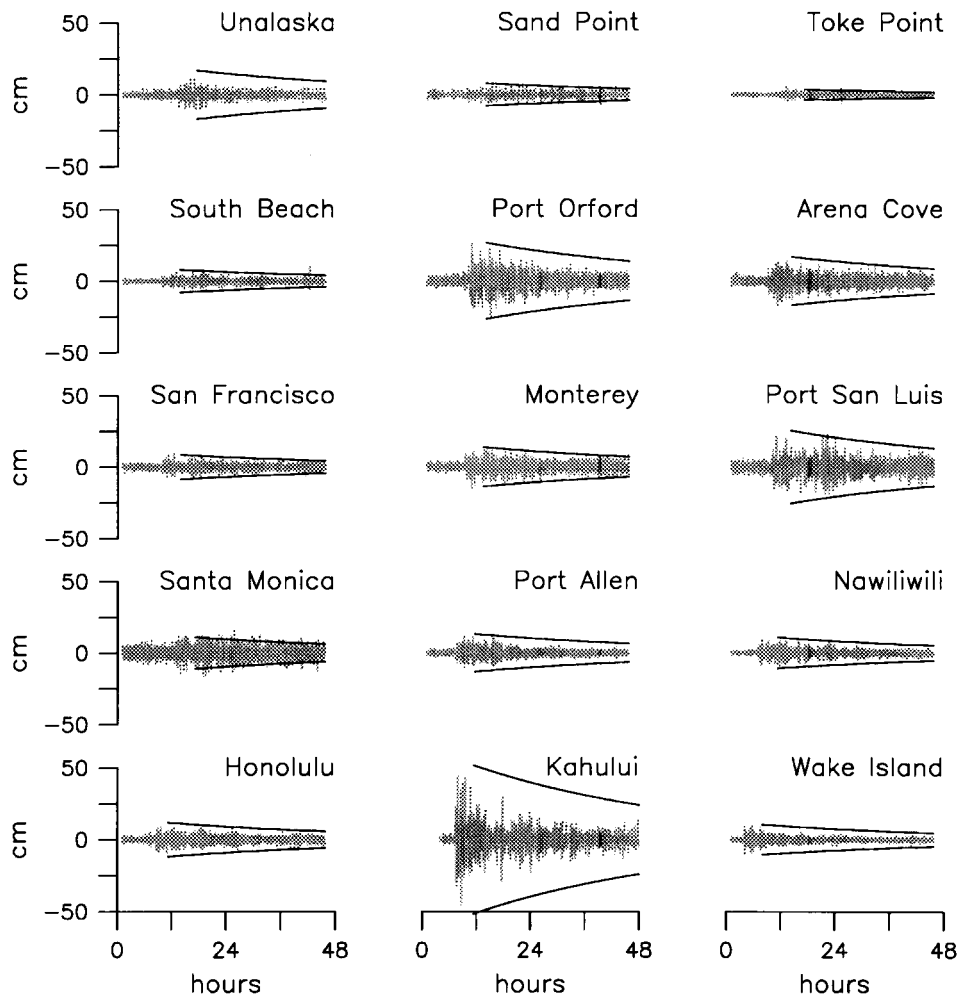


Figure 8. Wave height forecasts and detided observations for the 1994 Shikotan tsunami, as observed at selected U.S. sites. The locations of these sites are shown in Figure 7. Times are hours since the earthquake (1323 UTC 4 October 1994).

5. Discussion

The method described in this paper provides forecasts that begin 4 h after the local tsunami onset. To forecast the heights of earlier waves in a tsunami, a different approach is required. The latest high-resolution numerical models can provide such forecasts, when pre-computed simulations are quickly tuned to seismic and offshore tsunami gage data. One example of such a modeling approach is the MOST Project at PMEL (Titov and González, 1998; Titov *et al.*, 1999). The ac-

curacy of model forecasts begin to degrade after a few hours, exactly when the forecasts described in this paper become available. Hence, the two methods are complementary.

Numerical models will also be helpful in explaining why the statistical approach works during the first day of a tsunami, i.e., earlier than suggested by studies of tsunami energy decay (e.g., Miller *et al.*, 1962, Van Dorn, 1984, 1987). A heuristic argument can be made for the use of the statistical method for the first day. It is that the initial amplitudes of tsunamis are determined at the time of generation and that there is the tendency for tsunamis to have similar temporal patterns at a given tide gage. This argument is strong enough to justify a detailed modeling study to investigate the temporal behavior of tsunamis over several hours. This is in contrast to the usual goal of such models, which is to estimate the height, waveform and runup of the first few waves. Models will also be essential in determining factors relating tsunami wave heights at tide gages to other sites in the same region.

The focus of this paper has been on remotely generated tsunamis, which represent an important threat to Pacific coastal regions. However, locally generated tsunamis also threaten the coast. Examples of these are the destructive 1964 tsunami in Alaska and the 1975 tsunami in Hawaii (epicenters shown in Figure 5). While the 1992 Cape Mendocino tsunami was nondestructive, it illustrates that the first waves of a locally generated tsunami can be followed hours later by waves that have propagated slowly along the coast as edge waves (González *et al.*, 1995). Also of major concern are locally generated tsunamis in the Cascadia Subduction Zone, which generated a large tsunami along the Pacific Northwest Coast 300 years ago (see references in Mofjeld *et al.*, 1997a). Additional research is needed to see how to adapt the forecasting method to locally generated tsunamis.

6. Conclusions

A method has been developed to forecast later wave heights during Pacific-wide tsunamis. The forecasts are made for the vicinity of real-time reporting tide gages, which provide the data needed to make the forecasts. Each forecast consists of two envelopes: one for the highest wave peaks and a second for the lowest wave troughs. Both envelopes are modulated by the tides and include an exponential decay of tsunami wave heights with time. Formulas and algorithms for generating the forecasts are given in the text and the Appendix.

Reasonable forecasts (within 0.5 m) can be made when only 4 h have passed since local tsunami onset and apply to the remainder of the tsunami. This conclusion is based on probability theory, Monte Carlo analyses of synthetic tsunamis, and the study of observed tsunamis. The method should be helpful to emergency managers who guide rescue and recovery operations during Pacific-wide tsunamis.

Appendix

A.1. ALGORITHM FOR GENERATING TSUNAMI WAVE HEIGHT FORECASTS

To implement the forecast method, algorithms are necessary to automatically detect the local onset of a tsunami. The onset is detected by testing the difference between the water level observed η_{obs} and the background η_B against a threshold amplitude η_{thres}

$$|\eta_{\text{obs}} - \eta_B| \geq \eta_{\text{thres}}, \quad (7)$$

where the absolute magnitude is used because the first tsunami wave may be negative. The background water level η_B is the predicted tide for the tide gage, plus a running average over the past day of observed levels. The latter is used to include seasonal and intraseasonal fluctuations in the value of η_B , under the assumption that these low-frequency fluctuations do not change significantly during the tsunami event. The background level needs to be increased by a storm surge forecast whenever a winter storm or hurricane occurs during the tsunami event.

Once 4 h has passed since the local onset of the tsunami, the standard deviation σ of the tsunami-band fluctuations are computed from the formula

$$\sigma^2 = \frac{1}{n} \sum_{i=1}^n (\eta_{\text{obs}} - \eta_B)_i^2, \quad (8)$$

where η_B is computed for each time of observation and n is the number of tide gage observations within the 2-h time interval beginning 2 h after tsunami detection (e.g., $n = 120$ when the tide gage samples once a minute). The standard deviation σ is multiplied by the coefficient $A = 3.0$ to form the initial envelope amplitude η_o in (6). This amplitude is then multiplied by the exponential series $\exp[-(t - t_o)/\tau]$ that runs forward in time from the start of the forecast t_o . Here, the e -folding decay time is $\tau = 48$ h. Finally, the forecast of the background water level $\eta_B(t)$ is added $\pm \eta_e(t)$ to generate the forecast $\eta_F(t)$ for wave peaks and troughs, respectively. Wind waves and swell heights need to be included in the tsunami forecasts for exposed sites along the coast and for harbors subject to high wave action.

A.2. WAVELET METHOD FOR GENERATING SYNTHETIC TSUNAMI TIME SERIES

The synthetic tsunami time series in Section 2 were generated via the discrete wavelet transform (DWT). To generate a time series (e.g., Figure A1), we chose random values from a Normal distribution (Gaussian pdf with unit variance and zero mean) and placed them at locations in the amplitude vector corresponding to a single scale (frequency band); the amplitudes for all other scales were set to zero. After inverting the amplitude vector, the result was a stationary random time series that is band-limited in frequency. The least asymmetric LA10 wavelet was

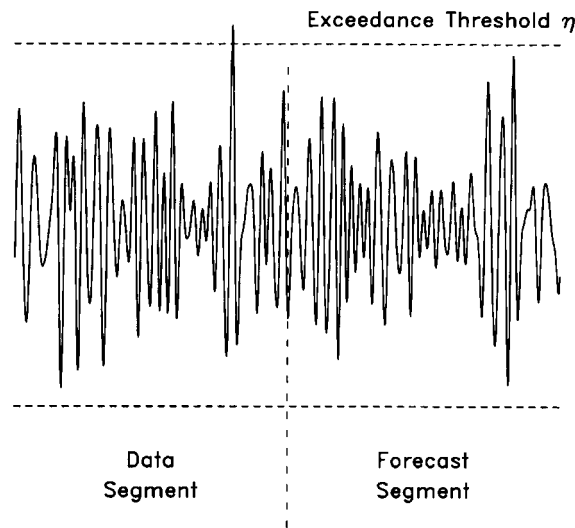


Figure A1. Example of a synthetic tsunami generated by wavelet methods, showing the data and forecast segments (equal length). Also shown is an exceedance threshold that is computed from the standard deviation σ in the data segment.

used because it yields fluctuations that are both relatively smooth and symmetric in time. The software routines used to generate the series are from Press *et al.* (1992), modified to use the LA10 wavelet.

Each series was divided into two segments of equal length (Figure A1): the data segment was then used to compute the standard deviation σ and a forecast segment used to compute the height distribution of the wave peaks and number of these exceeding the height $A\sigma$. The Monte Carlo simulations were done on sets of 1000 series (each 1024 values in length) for scales 8, 16 and 32. A large number of simulations were used for each case to provide reliable statistics for the extreme events in wave height. For consistency, the same 1000 series were used to analyze the behavior of the forecasts as function of the coefficient A . To establish confidence limits, each set was divided into five equal subsets. These limits were found to be ± 2 in the last digit of the numerical results that are shown in Section 2.

Acknowledgements

The authors wish to thank M. Moss, S. Gill and tidal observers (NOAA/National Ocean Service), as well as W. Van Dorn, for supplying tide gage data used in this study. Thanks as well to L. Mirth, E. Boss and M. Eble for digitizing mariograms and processing time series. This research was funded by the U.S. National Tsunami Hazard Mitigation Program, the Deputy Under Secretary of Defense for Space Integration, and the NOAA/Pacific Marine Environmental Laboratory. Con-

tribution No. 1884 from the NOAA/Pacific Marine Environmental Laboratory and Contribution No. 658 from the Joint Institute for the Study of the Atmosphere and Oceans.

References

- Cummins, P. R., Hirano, S., and Kaneda, Y.: 1998, Refined coseismic displacement modeling for the 1994 Shikotan and Sanriku-oki earthquakes, *Geophys. Res. Lett.* **25**(17), 3219–3222.
- Van Dorn, W. G.: 1984, Some tsunami characteristics deducible from tide records, *J. Phys. Oceanogr.* **14**(2), 353–363.
- Van Dorn, W. G.: 1987, Tide gage response to tsunamis. Part II: Other oceans and smaller seas, *J. Phys. Oceanogr.* **17**(9), 1507–1516.
- González, F. I., Satake, K., Boss, E. F., and Mofjeld, H. O.: 1995, Edge waves and non-trapped modes of the 25 April 1992 Cape Mendocino tsunami, *Pure Appl. Geophys.* **144**(3/4), 409–426.
- Lander, J. F. and Lockridge, P. A.: 1989, *United States Tsunamis (Including United States Possessions) 1690–1988*, NOAA NGDC Publ. 41-2, Boulder, CO.
- McGehee, D. D. and McKinney, J. P.: 1997, Tsunami detection and warning capability using nearshore submerged pressure transducers — Case study of the 4 October 1994 Shikotan tsunami, In: G. Hebenstreit (ed.), *Perspectives on Tsunami Hazard Reduction*, Kluwer, Norwell, MA, pp. 133–143.
- Miller, G. R., Munk, W. H., and Snodgrass, F. E.: 1962, Long-period waves over California's borderland. Part II: Tsunamis, *J. Mar. Res.* **20**(1), 31–41.
- Mofjeld, H. O.: 1992, Subtidal sea level fluctuations in a large fjord system, *J. Geophys. Res.* **97**(C12), 20,191–20,199.
- Mofjeld, H. O., Foreman, M. G. G., and Ruffman, A.: 1997a, West Coast tides during Cascadia subduction zone tsunamis, *Geophys. Res. Lett.* **24**(17), 2215–2218.
- Mofjeld, H. O., González, F. I., and Newman, J. C.: 1997b, Short-term forecasts of inundation during teletsunamis in the eastern North Pacific Ocean, In: G. Hebenstreit (ed.), *Perspectives on Tsunami Hazard Reduction*, Kluwer, Norwell, MA, pp. 145–155.
- Mofjeld, H. O., González, F. I., and Newman, J. C.: 1999, Tsunami prediction in U.S. Coastal Regions, In: C. Mooers (ed.), *Coastal Ocean Prediction*, AGU, Washington, D.C., pp. 353–375.
- Pacheco, J. and Sykes, L. R.: 1992, Seismic moment catalog of large shallow earthquakes, 1900 to 1989, *Bull. Seismol. Soc. Am.* **82**, 1306–1349.
- Percival, D. B. and Mofjeld, H. O.: 1997, Analysis of subtidal coastal sea level fluctuations using wavelets, *J. Am. Stat. Assoc.* **92**(439), 868–880.
- Press, W. H., Teukolsky, S. A., Vetterling, W. T., and Flannery, B. P.: 1992, *Numerical Recipes: The Art of Scientific Computing* (2nd edn), Cambridge, MA.
- Titov, V. V. and González, F. I.: 1999, *Implementation and Testing of the Method of Splitting Tsunami (MOST) Model*, NOAA Technical Memorandum ERL PMEL-112 (PB98-122773).
- Titov, V. V., Mofjeld, H. O., González, F. I., and Newman, J.: 1999, *Offshore Forecasting of AASZ Tsunamis in Hawaii*, NOAA Technical Memorandum ERL PMEL-114.
- Tanioka, Y., Ruff, L., and Satake, K.: 1995, The great Kurile earthquake of October 4, 1994 tore the slab, *Geophys. Res. Lett.* **22**(13), 1661–1664.

